

# Extremely large oblate deformation of the first excited state in $^{12}\text{C}$ : a new challenge to modern nuclear theory

C. Ngwetsheni<sup>a</sup>, J. N. Orce<sup>a,b</sup>, P. Navrátil<sup>c</sup>, P. E. Garrett<sup>a,d</sup>, T. Faestermann<sup>e</sup>, A. Bergmaier<sup>f</sup>,  
M. Frosini<sup>g</sup>, V. Bildstein<sup>d</sup>, B. A. Brown<sup>h</sup>, C. Burbadge<sup>d</sup>, T. Duguet<sup>i</sup>, K. Hadyńska-Klęk<sup>j</sup>,  
M. Mahgoub<sup>k,l</sup>, C. V. Mehl<sup>a</sup>, A. Pastore<sup>g</sup>, A. Radich<sup>d</sup>, S. Triambak<sup>a</sup>

<sup>a</sup>Department of Physics & Astronomy, University of the Western Cape, P/B X17, Bellville 7535, South Africa

<sup>b</sup>National Institute for Theoretical and Computational Sciences (NITheCS), South Africa

<sup>c</sup>TRIUMF, 4004 Wesbrook Mall, Vancouver, British Columbia V6T 2A3, Canada

<sup>d</sup>Department of Physics, University of Guelph, Guelph, Ontario N1G 2W1, Canada

<sup>e</sup>Physik Department, Technische Universität München, D-85748 Garching, Germany

<sup>f</sup>Institute for Applied Physics and Metrology, Universität der Bundeswehr München, D-85577 Neubiberg, Germany

<sup>g</sup>CEA, DES, IRESNE, DER, SPRC, F-13108 Saint Paul Lez Durance, France

<sup>h</sup>Department of Physics & Astronomy and National Superconducting Cyclotron Laboratory, Michigan State University, East Lansing, MI 48824-1321, USA

<sup>i</sup>IRFU, CEA, Université Paris-Saclay, 91191 Gif-sur-Yvette, France

<sup>j</sup>Department of Physics, University of Surrey, Guildford, GU2 7XH, UK

<sup>k</sup>Faculty of Science, Jazan University, Jazan, Saudi Arabia

<sup>l</sup>Faculty of Science, Sudan University of Science and Technology, Khartoum, Sudan

---

## Abstract

A Coulomb-excitation study of the high-lying first excited state at 4.439 MeV in the nucleus  $^{12}\text{C}$  has been carried out using the  $^{208}\text{Pb}(^{12}\text{C}, ^{12}\text{C}^*)^{208}\text{Pb}^*$  reaction at 56 MeV and the Q3D magnetic spectrograph at the Maier-Leibnitz Laboratorium in Munich. High-statistics achieved with an average beam intensity of approximately  $10^{11}$  ions/s together with state-of-the-art *ab initio* calculations of the nuclear dipole polarizability permitted the accurate determination of the spectroscopic quadrupole moment,  $Q_s(2_1^+) = +0.076(30)$  eb, in agreement with previous measurements. Combined with previous work, a weighted average of  $Q_s(2_1^+) = +0.090(14)$  eb is determined, which includes the re-analysis of a similar experiment by Vermeer and collaborators,  $Q_s(2_1^+) = +0.103(20)$  eb. Such a large oblate deformation challenges modern nuclear theory and emphasizes the need of  $\alpha$  clustering and associated triaxiality effects for full convergence of E2 collective properties.

**Keywords:** Coulomb excitation, *ab initio* calculations, photo-absorption cross section, dipole polarizability, spectroscopic quadrupole moment

---

## 1. Introduction

Advanced beam delivery, high-resolution and high-efficiency detectors in modern accelerator facilities permit the precise determination of electromagnetic properties involving high-lying excited states in light nuclei. Ergo the feasibility to benchmark modern theory from *ab initio* [1–4], beyond mean-field [5–7] and cluster-model [8–11] calculations. A suitable testing ground concerns the nucleus  $^{12}\text{C}$ , with a first excitation of angular momentum  $J^\pi = 2_1^+$  lying at 4.439 MeV.

Unlike excitation energies, electromagnetic transitions provide a more stringent test of the many-body Hamiltonian because they involve the overlap between initial and final wave functions. Particularly, the reduced transition probability between the ground  $0_1^+$  and first-excited  $2_1^+$  states — the  $B(E2; 0_1^+ \rightarrow 2_1^+) = |\langle 2_1^+ || \hat{E}2 || 0_1^+ \rangle|^2$  value — quantifies the collective motion through the  $\hat{E}2$  electric-quadrupole operator. This is precisely measured in  $^{12}\text{C}$ ,  $B(E2; 0_1^+ \rightarrow 2_1^+) = 0.00390(8) e^2 b^2$ , with a remarkable 2% uncertainty [12–28] in agreement with state-of-the-art *ab initio* calculations using large harmonic-oscillator basis sizes,  $N_{\text{max}}$  [13, 29, 30]. Albeit general concordance,

---

Email address: jnorce@uwc.ac.za (J. N. Orce)

Monte Carlo lattice calculations at leading order (LO) underestimate the experimental value [3], emphasizing the need of higher-power counting orders in chiral effective field theory ( $\chi$ EFT), i.e., the inclusion of three-nucleon (3N) forces and other non-local contributions to the nucleon-nucleon (NN) interaction [31].

The spectroscopic quadrupole moment of the first  $2_1^+$  state,  $Q_s(2_1^+)$ , is related to the diagonal matrix element of the  $\hat{E}2$  irreducible rank-2 tensor as

$$\begin{aligned} Q_s(2_1^+) &= \sqrt{\frac{16\pi}{5}} \frac{1}{\sqrt{2J+1}} \langle JJ20 | JJ \rangle \langle 2_1^+ || \hat{E}2 || 2_1^+ \rangle \\ &= 0.75793 \langle 2_1^+ || \hat{E}2 || 2_1^+ \rangle, \end{aligned} \quad (1)$$

and quantifies the ellipsoidal deformation of the charge distribution in the laboratory frame [32]. This value is known to a much lesser extent in  $^{12}\text{C}$  with only three measurements being performed [33–35]. The  $Q_s(2_1^+)$  value can be determined at energies well below the Coulomb barrier for states with  $J \neq 0, 1/2$  using the re-orientation effect (RE), which is a second-order effect in Coulomb-excitation perturbation theory that causes a distinct population of the magnetic substates depending on the deformation [36]. For the excitation probability of a  $0_1^+ \rightarrow 2_1^+$  transition in the projectile nucleus [32],

$$P_{02}^{(2)} = P_{02}^{(1)} + P_{02}^{(1,2)}, \quad (2)$$

where RE is accounted by the interference term  $P_{02}^{(1,2)}$ , which includes both E1 and E2 phenomena, adding to the first-order term  $P_{02}^{(1)} \propto B(E2; 0_1^+ \rightarrow 2_1^+)$ . The contribution of the RE in  $P_{02}^{(2)}$ ,  $r_p(\xi, \vartheta)$ , is given by [37],

$$r_p(\xi, \vartheta) = \frac{P_{02}^{(1,2)}(E2)}{P_{02}^{(1)}} \approx 1.32 \frac{A_p}{Z_p} \frac{\Delta E}{1 + A_p/A_T} Q_s(2_1^+) K(\xi, \vartheta), \quad (3)$$

where  $\Delta E$  is the  $2_1^+$  excitation energy,  $Z_p$  and  $A_p$  the charge and mass numbers of the projectile, respectively, and  $K(\xi, \vartheta)$  a function, with values ranging between 0.2 and 0.3 for this experiment [37], that depends on the scattering angle in the center-of-mass frame,  $\vartheta$ , and the adiabaticity parameter,  $\xi$ , given by the ratio between the collision time,  $\tau_{\text{collision}}$ , and the lifetime of the level  $\tau_{\text{level}} = \hbar/\Delta E$  [37]. For sudden-impact collisions,  $\xi \lesssim 1$ , while for adiabatic collisions,  $\xi \gg 1$ . A larger sensitivity to the RE is attained for large  $|Q_s(2_1^+)|$  values, large scattering angles where  $K(\xi, \vartheta)$  is maximized, and heavy targets,  $A_T$  [38].

An interesting correlation between  $B(E2; 0_1^+ \rightarrow 2_1^+)$  and  $Q_s(2_1^+)$  values is inferred from *ab initio* calculations in  $^{12}\text{C}$  [2, 13], where the extrapolated  $Q_s(2_1^+)$  value can be calculated precisely from the well-known

$B(E2; 0_1^+ \rightarrow 2_1^+)$  [13]. The largest basis size was  $N_{\text{max}} = 8$  [2, 30], where the importance-truncation No-Core Shell Model (IT- NCSM) [39] was used with the CD-Bonn 2000 NN potential [40] and a variety of 2N+3N chiral interactions [2]. Values of  $Q_s(2_1^+)$  ranging from 0.045 to 0.065 eb have been computed from the  $B(E2; 0_1^+ \rightarrow 2_1^+) - Q_s(2_1^+)$  correlation [2, 13]. A similar result of  $Q_s(2_1^+) \approx 0.06$  eb is determined by other *ab initio* [3, 4, 13, 30] and theoretical approaches [41, 42], including shell-model (SM) calculations using the Cohen-Kurath interaction [43] and admixtures outside the p-shell from the isoscalar giant quadrupole resonance [42]. Lastly, Monte Carlo lattice calculations [3] and cluster models [8–11] predict an oblate shaped  $2_1^+$  state in  $^{12}\text{C}$ , with a compact triangular three- $\alpha$  cluster and mean-field admixtures. Larger  $Q_s(2_1^+)$  values can certainly be calculated by the shell model using larger effective charges [44–46], as recently reviewed by Saiz and collaborators [35]. In this Letter we present a high-statistics RE measurement yielding the most accurate  $Q_s(2_1^+)$  value in  $^{12}\text{C}$  in agreement with previous Coulomb-excitation measurements [33–35]. When combined with prior work, an extremely large oblate deformation is determined in conflict with modern theoretical approaches.

## 2. Experiment Details

A safe Coulomb-excitation of the  $2_1^+$  state in  $^{12}\text{C}$  has been performed using the high resolution Q3D magnetic spectrograph at the Maier-Leibnitz-Laboratory (MLL) in Garching, Munich (Germany) [47]. Beams of  $^{12}\text{C}$  with an intensity of up to 10 pA with a  $5^+$  charge state were accelerated to  $T_{\text{lab}} = 56$  MeV by the Tandem Van de Graaff accelerator. A 99.36% enriched  $^{208}\text{Pb}$  target with 100  $\mu\text{g}/\text{cm}^2$  thickness was located at the object focus of the Q3D magnetic spectrograph [47]. The scattered  $^{12}\text{C}$  ions were momentum analyzed by the spectrograph, with the magnetic field such that  $^{12}\text{C}$  ions corresponding to the excitation of the high-lying states  $^{12}\text{C}(2_1^+)$  and  $^{208}\text{Pb}(4_1^+, 2_1^+, 3_1^-)$  states at 4.32 MeV, 4.09 MeV and 2.61 MeV, respectively, together with those elastically scattered reached the focal plane.

Reaction products enter the Q3D spectrograph through an aperture with a solid angle  $\Omega = 14$  msr and are focused vertically by the quadrupole magnet. The horizontal focusing onto the focal-plane detector is achieved by the dipole magnetic field, which separates the trajectories according to the ratio momentum/charge. The detector system is a combination of two aligned, 1-m long, gas filled proportional counters for position measurement using the signals from both

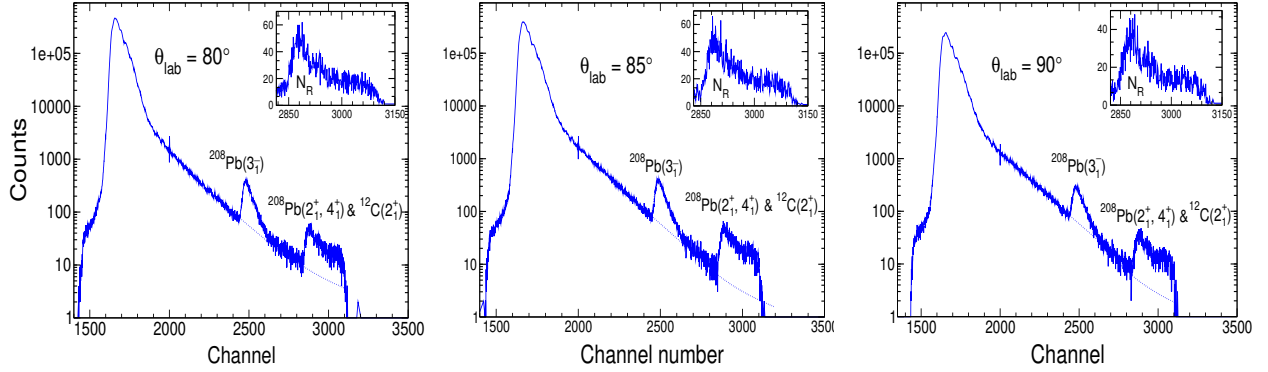


Figure 1: Particle energy spectra collected at  $80^\circ$  (left),  $85^\circ$  (middle) and  $90^\circ$  (right) scattering angles with 56 MeV  $^{12}\text{C}$  ions. All identified peaks are labelled and the blue dotted line represents the elastic peak line-shape. The inset shows an expanded spectrum with the broadened  $2_1^+$  peak in  $^{12}\text{C}$  overlapping with the  $2_1^+$  and  $4_1^+$  peaks in  $^{208}\text{Pb}$ .

sides of the wires and particle identification using energy losses  $\Delta E$  and a 1-m long Frisch-grid ionization chamber with an anode which has five strips, where five  $\Delta E$  plus the total energy ( $E$ ) are measured [48].

Data acquisition was carried out using the ROOT based MARABOU software [49]. The resulting particle spectra obtained at spectrograph angles of  $\theta = 80^\circ$  (left),  $85^\circ$  (middle) and  $90^\circ$  (right) are shown in Fig. 1. The spectra show the dominant elastic peak, prominent  $3_1^-$  peak in  $^{208}\text{Pb}$  and the broadened  $2_1^+$  peak in  $^{12}\text{C}$ , coinciding with the  $2_1^+$  and  $4_1^+$  peaks in  $^{208}\text{Pb}$  (insets in Fig. 1). The broadening of the peak due to the  $^{12}\text{C}$   $2_1^+$  state results from the emission of the 4.439 MeV  $\gamma$  ray while the  $^{12}\text{C}$  ions are in flight [50]. A similar particle spectrum was collected by Vermeer and collaborators [34], using a split-pole magnetic spectrograph, where scattered ions from  $T_{\text{lab}} = 53$  to 58 MeV were detected at  $90^\circ$  by a position-sensitive, multi-element proportional counter.

The semi-classical coupled-channel Coulomb-excitation code GOSIA [51] was used to simulate the corresponding population probabilities, where the semi-classical approximation (SCA) was satisfied with a Sommerfeld parameter of  $\eta = \frac{a}{\lambda} = 36 \gg 1$ , defined by the ratio between half the distance of closest approach in a head-on collision,  $a$ , and the de Broglie wavelength  $\lambda$  [32]. Concurring results shown below indicate that nuclear effects are negligible at  $\theta = 80^\circ$ ,  $85^\circ$  and  $90^\circ$ , which correspond to separations between nuclear surfaces of  $S(\vartheta) = 6.5$ , 6.0 and 5.6 fm, respectively, where,

$$S(\vartheta) = \frac{1.44 Z_p Z_T}{2T_{\text{lab}}} (1 + A_p/A_T) [1 + \text{cosec}(\vartheta/2)] - 1.25(A_p^{1/3} + A_T^{1/3}) \text{ fm}, \quad (4)$$

The SCA is further supported by a similar RE study [34], where the safe bombarding energy was measured at  $90^\circ$ , finding consistent results at  $T_{\text{lab}} = 53$ , 54 and 56 MeV, with an onset of nuclear interference at 58 MeV [34].

### 3. Data Analysis

The extraction of the  $Q_s(2_1^+)$  value depends on the excitation probabilities from experimental data and those calculated by GOSIA [51]. Prior determination of the experimental excitation probabilities requires background subtraction of the elastically scattered  $^{12}\text{C}$  ions. Here, the background subtraction was done using the line shape of the elastic peak, denoted by the fine dotted line in Fig. 1. The line shape can be fitted with an exponential or a Landau function, and the best fit is selected based on the minimum mean square error. Spreading of the  $^{208}\text{Pb}(3_1^-)$  peak may affect the elastic peak line shape and ultimately the background subtraction of the broadened peak area  $N_R$  (insets in Fig. 1). This was investigated by fitting the  $^{208}\text{Pb}(3_1^-)$  peak with a Landau function extending to the peripheral of  $N_R$  and compared with the exponential function fitting the elastic peak line shape, resulting in a difference of 1.8% at  $80^\circ$ , 7.8% at  $85^\circ$  and 5.6% at  $90^\circ$  in the statistics of  $N_R$  after background subtraction, which is included in the uncertainties of  $N_R$ . The peak counts after background subtraction are then used to calculate the experimental population probabilities, i.e.,

$$P(^{12}\text{C}; 2_1^+) = \frac{N(^{12}\text{C}; 2_1^+)}{N_{\text{total}}}, \quad (5)$$

where  $N_{\text{total}}$  is the total number of counts recorded, including  $N(^{12}\text{C}; 2_1^+)$ .

The region  $N_R$  includes the peak due to the  $^{12}\text{C}$   $2_1^+$  as well as contributions from the excited states in  $^{208}\text{Pb}$ , namely the  $2_1^+$  and  $4_1^+$  states. These latter contributions must be subtracted, and this was accomplished using the GOSIA calculated population probabilities,  $P(^{208}\text{Pb}; 2_1^+, 4_1^+)$ , as  $N(^{12}\text{C}; 2_1^+) = N_R - N_{\text{total}}P(^{208}\text{Pb}; 2_1^+, 4_1^+)$ . Table 1 shows statistics and populations of the  $^{12}\text{C}(2_1^+)$  state, where the reported uncertainties include statistical and systematic uncertainties from the background subtraction procedure. We also investigated the impact of the E1 transition  $\langle 3_1^- || \hat{E}1 || 2_1^+ \rangle$  on  $P(^{208}\text{Pb}; 2_1^+)$ , which is negligible  $\approx 0.3\%$ .

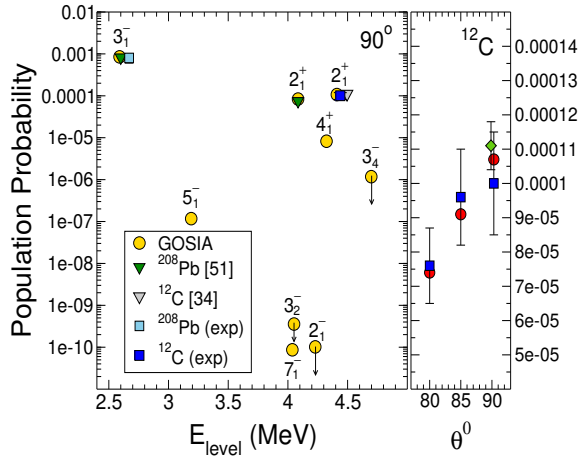


Figure 2: (Left panel) Calculated (circles) and measured (squares) population probabilities on a logarithmic scale for  $^{208}\text{Pb}$  states and  $^{12}\text{C}(2_1^+)$ , respectively, at  $90^\circ$ . The right panel also shows calculated (circles) and measured (squares) population probabilities on a linear scale for  $^{12}\text{C}$  versus scattering angle  $\theta$ . The previously measured population probabilities of  $^{12}\text{C}(2_1^+)$  [34] and  $^{208}\text{Pb}(3_1^-, 2_1^+)$  states [52] (triangles down) are shown for comparison.

Figure 2 presents the population probabilities of all levels in the energy range of interest for both  $^{12}\text{C}$  and  $^{208}\text{Pb}$ . Our experimental results (squares) are in agreement with preceding measurements by Vermeer and co-workers at  $90^\circ$  (triangles down) [34, 52] for the  $2_1^+$  and  $3_1^-$  states in  $^{12}\text{C}$  and  $^{208}\text{Pb}$ , respectively. A value of  $B(E3; 0_1^+ \rightarrow 3_1^-) = 0.583(18) e^2 b^3$  has been determined for  $^{208}\text{Pb}$  in agreement with previous work [53, 54]. The arrows pointing down in Fig. 2 are upper limits assuming a dominant E2 transition, where there is likely M1/E2 admixtures. The population of  $^{208}\text{Pb}(3_2^-, 3_4^-)$  states may contribute to the counts in the region  $N_R$ , and must also be accounted for. Both states contribute insignificantly to  $N_R$ , the largest being the  $3_4^-$  state with a maximum of 48 counts. The resulting population of

the  $^{12}\text{C}(2_1^+)$  state has a sensitivity to both the  $0_1^+ \rightarrow 2_1^+$  transition and the  $2_1^+$  diagonal matrix elements, but also is sensitive to the polarizability of the  $^{12}\text{C}$  states. This polarizability must be accurately accounted for in the excitation process.

	$80^\circ$	$85^\circ$	$90^\circ$
$N(^{12}\text{C}; 2_1^+)$	2837(412)	3157(447)	2157(320)
$10^5 \times P(^{12}\text{C}; 2_1^+)$	7.6(1.1)	9.6(1.4)	10.0(1.5)

Table 1: The statistics of the  $^{12}\text{C} 2_1^+$  peak and populations.

#### 4. Dipole Polarizability

A competing phenomenon in the determination of  $Q_S(2_1^+)$  values in light nuclei is the E1-polarizability, which must be corrected for in Coulomb-excitation codes [51]. The E1 polarization correction arises from virtual excitations of giant dipole resonance (GDR) states, which polarize the final excited level via the two-step process:  $|i\rangle \rightarrow |n\rangle \rightarrow |f\rangle$  or  $0_1^+ \rightarrow 1_{\text{GDR}}^- \rightarrow 2_1^+$ , for the general case of an even-even nucleus. Previous studies show that E1-polarizability corrections are necessary in order to reproduce the excitation probabilities measured for the  $J = 1/2$  first excited levels in  $^7\text{Li}$  and  $^{17}\text{O}$  [55–57], where  $Q_S(J = 1/2) = 0$  and the E1 polarizability is the only second-order effect. This is included in the effective quadrupole interaction by the dimensionless polarizability parameter  $\kappa$ , which measures deviations between the actual effects from the GDR and the hydrodynamic model [58]. The value of  $\kappa(0_1^+)$  can be determined from the  $(-2)$  moment of the total photo-absorption cross section,  $\sigma_{-2}$  [58, 59],

$$\sigma_{-2} = \int_0^{E_\gamma} \frac{\sigma_{\text{total}}(E_\gamma)}{E_\gamma^2} dE_\gamma = 2.38 \kappa A^{5/3} \mu\text{b}/\text{MeV}. \quad (6)$$

As mentioned before, the interference term  $P_{02}^{(1,2)}$  entails an E1 component. Similar to Eq. 3, the GDR effect can be approximated by [37]

$$d_p(\xi, \vartheta) = \frac{P_{02}^{(1,2)}(E1)}{P_{02}^{(1)}} \approx -7.37 \frac{T_{\text{lab}} \sigma_{-2}}{(1 + A_p/A_t) Z_t Z_t R^2} \phi(\xi, \vartheta), \quad (7)$$

where  $\phi(\xi, \vartheta)$  also contains kinematical information and varies between approximately 0.03 and 0.1 [37] and  $R = 1.25 A^{1/3}$  fm is the spherical nuclear radius. Ultimately, we can approximate the second-order excitation probability by the sum,  $P_{02}^{(2)} = P_{02}^{(1)} [1 + r_p(\xi, \vartheta) +$

$d_p(\xi, \vartheta)$ ]. However, there is currently no experimental data of  $\sigma_{-2}$  or  $\kappa$  values for excited states in even-even nuclei. Recent developments using the formalism of Häusser and collaborators [55] based on E1 and E2 matrix elements, second-order perturbation theory and the hydrodynamic model, show that  $\sigma_{-2}(2_1^+)$  and  $\kappa(2_1^+)$  can be calculated as [60]

$$\sigma_{-2}(2_1^+) = 0.6 \frac{ZA^{2/3}S(E1)}{\langle 0_1^+ \parallel \hat{E}2 \parallel 2_1^+ \rangle} \text{ fm}^2/\text{MeV}, \quad (8)$$

$$\kappa(2_1^+) = \frac{1}{0.00039 \frac{A}{Z}} \frac{S(E1)}{\langle 0_1^+ \parallel \hat{E}2 \parallel 2_1^+ \rangle}, \quad (9)$$

for the two-step process,  $0_1^+ \rightarrow 1_{\text{GDR}}^- \rightarrow 2_1^+$ , where Eqs. 8 and 9 satisfy Eq. 6 and  $S(E1)$  is defined as

$$S(E1) := \frac{1}{2J_i + 1} \sum_{J_n, \Delta T} W_{\text{inf}} \frac{\langle i \parallel \hat{E}1 \parallel n \rangle \langle n \parallel \hat{E}1 \parallel f \rangle}{E_\gamma}, \quad (10)$$

in units of  $e^2 \text{fm}^2/\text{MeV}$ , where the sum considers all intermediate states  $|n\rangle = |1_{\text{GDR}}^- \rangle$  connecting both the initial  $|i\rangle = |0_1^+ \rangle$  and final  $|f\rangle = |2_1^+ \rangle$  states via isovector E1 transitions — following the isospin selection rule  $\Delta T = 1$  for  $N = Z$  self-conjugate nuclei [61] — and  $W_{\text{inf}} = W(1102, 21)$  is the corresponding Racah W-coefficient [62]. Consequently,  $\sigma_{-2}(2_1^+)$  and  $\kappa(2_1^+)$  values can be determined from theoretical models by computing E1 and E2 matrix elements. The calculated  $\kappa(2_1^+)$  value is then input in GOSIA [51] for further analysis.

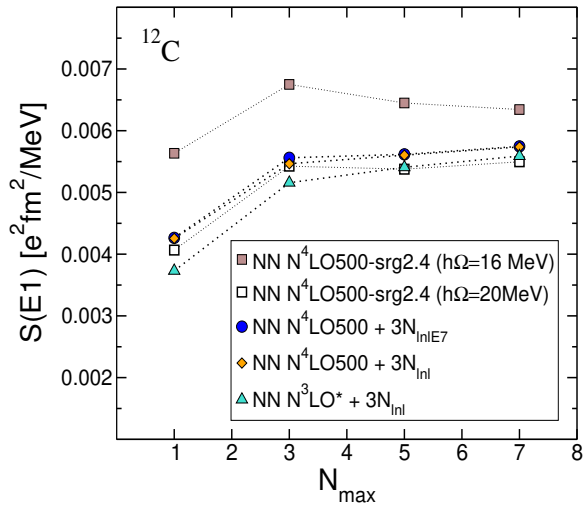


Figure 3: Calculated sum of E1 matrix elements ( $S(E1)$  in Eq. 10) using the NCSM and different  $\chi$ EFT interactions over all intermediate states  $|J_n\rangle = |1_{\text{GDR}}^- \rangle$  connecting both  $|0_1^+ \rangle$  and  $|2_1^+ \rangle$  states. The frequencies used for the  $N^4$ LO interactions were  $\hbar\Omega = 18$  MeV while for  $N^3$ LO  $\hbar\Omega = 20$  MeV unless otherwise specified in the legend.

In the present work  $\kappa(2_1^+)$  has been calculated using the *ab initio* NCSM method with the Similarity Renormalization Group (SRG) evolved [63] non-local  $\chi$ EFT NN interaction, NN  $N^4$ LO500-srg2.4 [1, 64], employed in our previous study [33], as well as with three  $\chi$ EFT interactions, also SRG evolved, that include 3N forces; namely, NN  $N^3$ LO\* +  $3N_{\text{inl}}$  [65, 66], NN  $N^4$ LO +  $3N_{\text{inl}}$  [64, 67], and the recently developed NN  $N^4$ LO +  $3N_{\text{inl}}^*$  interaction [64, 68, 69], which contains a sub leading 3N contact term (E7) that enhances the strength of the spin-orbit interaction [69]. The latter is the interaction that better predicts the excitation energy,  $E(2_1^+) = 4.1$  MeV (4.44 MeV experimentally). The NCSM calculations have been performed in basis spaces ranging from  $N_{\text{max}} = 0/1$  to  $N_{\text{max}} = 6/7$ , where the odd  $N_{\text{max}}$  spaces were used for the intermediate  $1^-$  states and even  $N_{\text{max}}$  for the  $0_1^+$  and  $2_1^+$  states, with the odd  $N_{\text{max}}$  calculation matched with the even  $N_{\text{max}} - 1$  calculation. We implemented the Lanczos continued fraction algorithm (LA) method [70] to perform exactly the summation over the intermediate  $1_{\text{GDR}}^-$  states in Eq. 10. The NCSM-LA method allows to account for the gamma strength well above 30 MeV that was the limit we reached in the previous NCSM calculations with the intermediate states explicitly computed, e.g., 28 states in  $N_{\text{max}} = 6/7$  [33]. Only in the  $N_{\text{max}} = 0/1$  space, we can calculate all the  $1^-$  states (248) and perform the sum 10 explicitly. The result then serves as a benchmark for the LA method. We note that no effective charges are used in the NCSM calculations.

In Fig. 3, we present the dependence of  $S(E1)$  (10) on the basis size  $N_{\text{max}}$  for all the used chiral interactions. We find a good convergence that allows a robust inference of  $S(E1) = 0.0060(5) e^2 \text{fm}^2/\text{MeV}$ . This result is slightly higher but still consistent with the calculation reported in Ref. [71]. We note that a good convergence of  $S(E1)$  is consistent with other NCSM-LA calculations of various observables that involve a Green's function, including anapole and electric dipole moments [72–74]. This is in contrast to a slow convergence of observables sensitive to the wave function tail such as the quadrupole moments and radii. Consequently, in order to obtain a robust prediction for  $\kappa(2_1^+)$ , we use the experimental value of the matrix element  $\langle 0_1^+ \parallel \hat{E}2 \parallel 2_1^+ \rangle = 6.247(63) \text{ efm}^2$  (or  $B(E2; 0_1^+ \rightarrow 2_1^+) = 39.0(8) e^2 \text{fm}^4$ ) in Eq. 8, yielding  $\kappa(2_1^+) = 1.2(1)$ . We also computed  $\kappa(0_1^+) = 1.8(1)$  within the NCSM-LA approach, which is consistent with the experimental value of  $\kappa(0_1^+) = 1.6(2)$  arising from Fuller's corrections [75] to the overestimated photo-absorption cross-section data by Ahrens and co-workers [76].

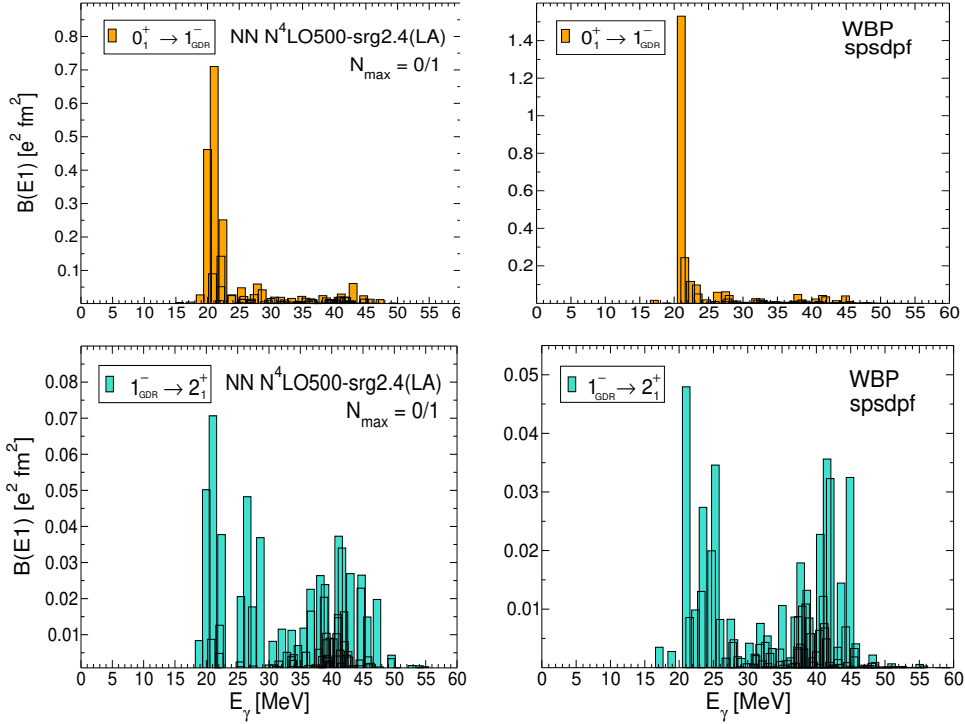


Figure 4: The  $B(E1)$  strengths calculated using the NN  $N^4$ LO500-srg2.4 with  $N_{\max} = 0/1$  (left panels) and WBP (right panels) interactions for the transitions  $0_1^+ \rightarrow 1_{\text{GDR}}^-$  (top) and  $1_{\text{GDR}}^- \rightarrow 2_1^+$  (bottom).

The present  $\kappa(2_1^+)$  value is lower than that obtained in Ref. [33] for two reasons: (i) All  $1_{\text{GDR}}^-$  states have been included to compute  $S(E1)$  in the present study by the LA method contrary to just 28 states computed explicitly in [33]. It turns out that the higher-lying states above the main GDR peak contribute destructively to  $S(E1)$ . This is consistent with calculations reported in Ref. [71]. We have verified this explicitly in the  $N_{\max} = 0/1$  calculations shown in the left panels of Fig. 4 (note that only the  $B(E1)$  values connecting the  $0_1^+$  and  $2_1^+$  states to the  $1_{\text{GDR}}^-$  states are shown, not the  $S(E1)$  contributing terms). (ii) We use the experimental value of  $\langle 0_1^+ || \hat{E}2 || 2_1^+ \rangle$ , which is larger than the NCSM ones in the  $N_{\max}$  spaces employed here and in Ref. [33]. The obtained  $\kappa(2_1^+)$  value is in line with what is found in other self-conjugate nuclei in the psd shells [60, 77]. The left panels of Fig. 4 also reveal the weak coupling between the  $2_1^+$  and  $1_{\text{GDR}}^-$  states.

Further SM calculations using the phenomenological WBP interaction [78] in the spsdpf model space with effective charges  $e_p = 1.275$  and  $e_n = 0.275$  [42, 44] yields  $B(E2; 0_1^+ \rightarrow 2_1^+) = 0.004254 e^2 b^2$ , in agreement with experiment [12, 79], and  $Q_s(2_1^+) = 0.0623$  eb. Additionally, the WBP interaction predicts a slightly smaller

$\kappa(2_1^+) = 0.9$  and larger  $\kappa(0_1^+) = 3.2$  values. As shown in the right panels of Fig. 4, the distribution of E1 strength up is less fragmented than the NCSM calculation and concentrated at 21 MeV for the  $0_1^+ \rightarrow 1_{\text{GDR}}^-$  calculation, which is lower than the experimental  $E_{\text{GDR}} \approx 24$  MeV [75]. We note that the WBP interaction estimates a binding energy of 102.36 MeV for the ground states, that is  $\approx 10$  MeV larger than the measured 92.16 MeV [80].

## 5. Results and Discussion

Empirically, the  $Q_s(2_1^+)$  value is determined utilizing population probabilities. In a combined analysis using the sum of the populations of all angles, we performed a least squares search by varying  $\langle 2_1^+ || \hat{E}2 || 2_1^+ \rangle$  until the population probabilities calculated by GOSIA converge with the experimental value determined by Eq. 5. The least squares is described by

$$X_i = \frac{[P(^{12}\text{C}; 2_1^+) - P_i(\langle 2_1^+ || \hat{E}2 || 2_1^+ \rangle)]^2}{\sigma_p^2}, \quad (11)$$

where  $\sigma_p$  is the uncertainty of  $P(^{12}\text{C}; 2_1^+)$  and  $P_i$  is the population probability from GOSIA, whose mag-

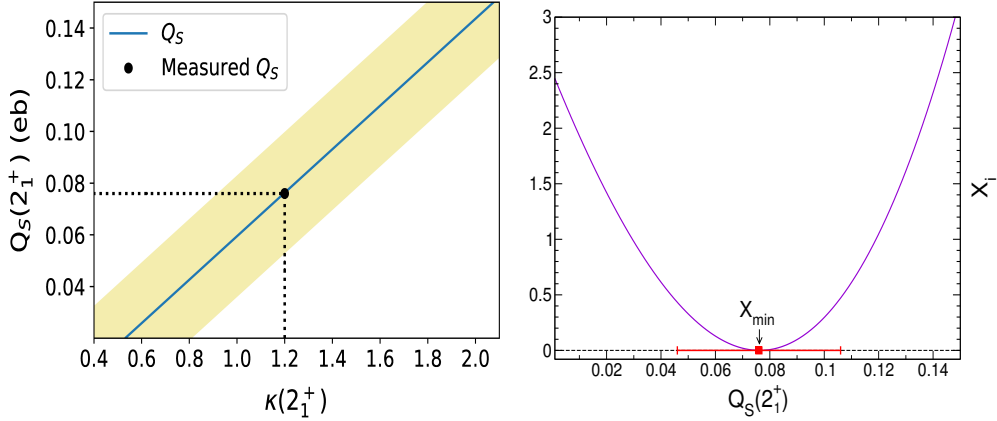


Figure 5: (Left panel) General trend of the extracted  $Q_s(2_1^+)$  by fitting population probabilities from GOSIA as a function of  $\kappa$ . The shaded band represent the uncertainty region. (Right panel) The  $X_i$  curve obtained from the least squares search and the red data point with an error bar corresponds to the measured  $Q_s(2_1^+)$ .

nitude varies with  $\langle 2_1^+ \parallel \hat{E}2 \parallel 2_1^+ \rangle$ . Convergence of the probabilities is reached at a global minimum  $X_{\min} = 0$ , where  $P(^{12}\text{C}; 2_1^+) = P_1$ . The right panel of Fig. 5 presents the  $X_i$  curve of our analysis as a function of the assumed  $Q_s(2_1^+)$  value. The  $X_{\min}$  corresponds to  $Q_s(2_1^+) = 0.076(30)$  eb, which is the quoted measurement in this work. Uncertainty of the latter stems from the statistical uncertainty determined by finding the value of  $Q_s(2_1^+)$  corresponding to  $P(^{12}\text{C}; 2_1^+) \pm \sigma_p$  in the GOSIA analysis, and phenomenological effects, i.e., high-lying  $2_2^+$  and  $0_2^+$  states in  $^{12}\text{C}$ , quantal effects and the  $\kappa(2_1^+)$  value. The  $2_2^+$  and  $0_2^+$  states have negligible effect on our measurement  $\sim 0.4 \times 10^{-3}$  eb. In order to ascertain the confidence levels of the SCA in support of our argument regarding the “safety” of the experiment, quantum effects whose magnitude is proportional to  $1/\eta = 1/38$  ( $\sim 2.6\%$ ), must be added to the uncertainty. Another vital parameter is the fixed transitional matrix element in GOSIA;  $\langle 0_1^+ \parallel \hat{E}2 \parallel 2_1^+ \rangle = 0.06247(63)$  eb. Lastly, the  $\kappa(2_1^+) = 1.2(1)$  value taken as input in GOSIA, is the only model dependent parameter. Therefore, we have investigated the correlation of  $\kappa(2_1^+)$  and  $Q_s(2_1^+)$ , as shown in the left panel of Fig. 5. It is clear that increasing  $\kappa(2_1^+)$  induces a larger oblate deformation. From the observed correlation, the uncertainty on  $\kappa(2_1^+)$  affects  $Q_s(2_1^+)$  by 0.003 eb. A summary of our results is presented in Table 2.

As shown in the right panel of Fig. 5, our result is within errors in concurrence with the large oblate deformation determined in previous RE measurements [33–35]. It is worth noting the analogous experiment by Vermeer and co-workers [34], where

Model	$B(E2; 0_1^+ \rightarrow 2_1^+)$ $e^2b^2$	$Q_s(2_1^+)$ eb	$\kappa(0_1^+)$	$\kappa(2_1^+)$
Shell Model	0.00425	0.0623	3.23	0.9
PGCM	0.00406	0.057	–	–
NCSM-LA	–	–	1.8(1)	1.2(1)
Rigid rotor	–	0.0566(6)	–	–
Experiment	0.00390(8) [12, 13]	0.076(30)*	1.6(2) [75]	–

Table 2: Theoretical model predictions of dipole and quadrupole parameters compared with experiment data. Calculations were performed using the WBP interaction [78] with the shell model, the  $N^2\text{LO EM1.8}/2.0$  interaction [81] with the PGCM, and four chiral interactions (NN  $N^4\text{LO500-srg2.4}$  [1, 64], NN  $N^3\text{LO}^* + 3N_{\text{nl}}$  [65, 66], NN  $N^4\text{LO} + 3N_{\text{nl}}$  [64, 67] and the recently developed NN  $N^4\text{LO} + 3N_{\text{nl}}^*$  interaction [64, 68, 69] with the NCSM-LA. The NCSM values for  $B(E2; 0_1^+ \rightarrow 2_1^+)$  and  $Q_s(2_1^+)$  are not shown as they are far from convergence in the accessible  $N_{\text{max}}$  spaces, see Fig. 6. The rigid rotor value is given by  $Q_s(2_1^+) = -\frac{2}{7} \left( \frac{16\pi}{5} B(E2; 0_1^+ \rightarrow 2_1^+) \right)^{1/2} = 0.9059 B(E2; 0_1^+ \rightarrow 2_1^+)^{1/2}$  [82, 83]. An asterisk indicates the  $Q_s(2_1^+)$  value arising from this work.

a reported value of  $Q_s(2_1^+) = 0.06(3)$  eb was determined for  $\kappa(2_1^+) = 0.68$  (i.e.,  $\kappa(2_1^+) = 1$  using Levinger’s  $\sigma_{-2} = 3.5 \kappa A^{5/3}$   $\mu\text{b}/\text{MeV}$  superseded formula [59], instead of Eq. 6). A re-analysis of this prior work using the currently more accurate weighted average,  $B(E2; 0_1^+ \rightarrow 2_1^+) = 0.00390(8) e^2b^2$  vs  $B(E2; 0_1^+ \rightarrow 2_1^+) = 0.00388(22) e^2b^2$  [34] — which includes all previous measurements [12, 13] — and the newly calculated  $\kappa(2_1^+) = 1.2(1)$  yields a larger and more precise value of  $Q_s(2_1^+) = 0.103(20)$  eb. Additionally, a recent result by Saiz-Lomas and co-workers [35] yields a larger  $Q_s(2_1^+) = 0.093_{-3.8}^{+3.5}$  eb using  $\kappa(2_1^+) = 1.0(2)$  and the high-

precision lifetime measurement [13], in agreement with the present work. Combining this and previous work, a weighted average of  $Q_S(2_1^+) = 0.090(14)$  eb is determined, which clearly challenges modern nuclear theory.

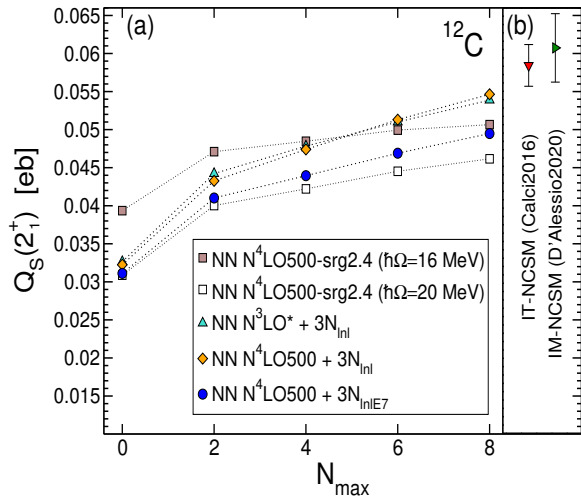


Figure 6: Panel (a) shows  $Q_S(2_1^+)$  values calculated with the NCSM as a function of  $N_{\max}$  using four different  $\chi\text{EFT}$  interactions. Panel (b) presents extrapolated  $Q_S(2_1^+)$  values obtained by Calci *et al.* [2] and D'Alessio *et al.* [13] from a  $B(E2;2_1^+ \rightarrow 0_1^+) - Q_S(2_1^+)$  correlation.

In panel (a) of Fig. 6, we present NCSM calculations of  $Q_S(2_1^+)$  obtained with the four chiral interactions used to compute  $S(E1)$  (shown in Fig. 3). The calculations have been performed in model spaces up to  $N_{\max} = 8$  without any further truncation. For the NN  $N^4\text{LO500-srg2.4}$ , results are shown for two frequencies,  $\hbar\Omega = 16$  MeV (upper line) and  $\hbar\Omega = 20$  MeV (lower line) yielding  $Q_S(2_1^+) \approx 0.05$  eb. However, the  $Q_S(2_1^+)$  values obtained with the more realistic chiral NN+3N interactions are clearly far from convergence. In panel (b), we show  $Q_S(2_1^+)$  values calculated from a correlation of  $Q_S(2_1^+)$  and  $B(E2;2_1^+ \rightarrow 0_1^+)$  values by Calci *et al.* [2] and D'Alessio *et al.* [13] using different chiral interactions and momentum cut-off parameter,  $\Lambda$ , yielding results of  $Q_S(2_1^+) \approx 0.06$  eb. These studies [2, 13] also reveal that  $Q_S(2_1^+)$  is insensitive to  $\Lambda$ .

The most likely explanation for the larger oblate deformation found in this work concerns  $\alpha$ -cluster effects that are not properly included in the NCSM. In fact, the degree of  $\alpha$  clustering in  $^{12}\text{C}$  has been investigated within the Fermionic Molecular Dynamics (FMD) and microscopic  $\alpha$ -cluster models [9], showing that the ground and  $2_1^+$  states present considerable  $\alpha$ -cluster triangle admixtures of 52% and 67%, respectively. Further, GDR states mainly arise from coherent

1-particle-1-hole (1p-1h) excitations, and  $\alpha$  clustering may not affect the NCSM calculations of E1 matrix elements in order to extract the dipole polarizability. However, an interesting work by He and collaborators shows that  $\alpha$  configurations may affect nuclear collective motion, specifically the GDR excitation, giving rise to a highly fragmented GDR spectrum [84]. The explicit account of deformation properties with chiral interaction can be efficiently probed via the projected generator coordinate method (PGCM) [85, 86]. This method mixing mean-field solutions with different deformations and orientations has been shown to incorporate efficiently long-range correlations. A PGCM calculation restricted to axially symmetric shapes and performed at  $N_{\max} = 11$  with EM1.8/2.0 Chiral interaction [81] yields  $E(2_1^+) = 4.2$  MeV,  $B(E2;0_1^+ \rightarrow 2_1^+) = 0.00406$   $e^2b^2$  and  $Q_S(2_1^+) = 0.057$  eb. While the first two observables are well reproduced, the too low spectroscopic quadrupole moment calls for triaxial configurations to account for triangle  $\alpha$  structures in  $^{12}\text{C}$  ground-state band.

## 6. Conclusions

In summary, we present a measurement of  $Q_S(2_1^+) = +0.076(30)$  eb in  $^{12}\text{C}$  by Coulomb excitation using the  $^{208}\text{Pb}(^{12}\text{C}, ^{12}\text{C}^*)^{208}\text{Pb}^*$  reaction at a safe energy of 56 MeV and the Q3D magnetic spectrograph positioned at angles  $80^\circ$ ,  $85^\circ$  and  $90^\circ$ . The analysis was carried out using population probabilities from GOSIA, assuming  $\kappa(2_1^+) = 1.2(1)$  determined from NCSM (using four chiral interactions) and the  $B(E2;0_1^+ \rightarrow 2_1^+) = 0.00390(8)$   $e^2b^2$  weighted value. Combined with previous work a large oblate deformation of  $Q_S(2_1^+) = +0.090(14)$  eb is determined, which challenges the rigid-rotor model at the  $1.3\sigma$  level as well as modern state-of-the-art *ab initio* calculations. Larger and untruncated harmonic oscillator basis sizes ( $N_{\max} > 10$ ) (or explicit introduction of  $\alpha$ -clusters [87, 88]) and possibly higher leading-order  $\chi\text{EFT}$  interactions [3, 89, 90] are probably required to include  $\alpha$ -clustering effects, and, particularly for  $^{12}\text{C}$ , the explicit inclusion of triaxiality, for convergence of E2 properties. The latter is a problem faced by the  $\chi\text{EFT}$  community with a particular challenge of determination of low-energy constants for the 3N force at 5<sup>th</sup> order [69]. Moreover, this work sheds light onto the impact of large  $\kappa$  values on E2 properties, particularly in low mass nuclei, and further calls for dedicated Coulomb-excitation measurements of the nuclear dipole polarizability in order to disentangle the RE and E1-polarizability effects in even-even nuclei, a research ground that remains practically untouched.

## Declaration of competing interest

There are no known competing financial interests or personal relationships that could have appeared to influence the work reported in this paper.

## Acknowledgements

This work was supported by the National Research Foundation (NRF) of South Africa under Grant 93500 and by the NSERC Grant No. SAPIN-2022-00019. TRIUMF receives federal funding via a contribution agreement with the National Research Council of Canada. Computing support came from an INCITE Award on the Summit and Frontier supercomputers of the Oak Ridge Leadership Computing Facility (OLCF) at ORNL, LLNL LC, and from the Digital Research Alliance of Canada. We also acknowledge the CEASINET project and the CCRT HPC resource (TOPAZE supercomputer) for PGCM calculations. We finally thank the late B. Singh for providing relevant information and M. Zielińska for contributions during and after the experiment.

## References

- [1] D. R. Entem, N. Kaiser, R. Machleidt, Y. Nosyk, Peripheral nucleon-nucleon scattering at fifth order of chiral perturbation theory, *Phys. Rev. C* 91 (1) (2015) 014002.
- [2] A. Calci, R. Roth, Sensitivities and correlations of nuclear structure observables emerging from chiral interactions, *Phys. Rev. C* 94 (1) (2016) 014322.
- [3] E. Epelbaum, H. Krebs, T. A. Lähde, D. Lee, U.-G. Meißner, Structure and rotations of the Hoyle state, *Phys. Rev. Lett.* 109 (25) (2012) 252501.
- [4] A. C. Dreyfuss, K. D. Launey, T. Dytrych, J. P. Draayer, C. Bahri, Hoyle state and rotational features in  $^{12}\text{C}$  within a no-core shell-model framework, *Phys. Lett. B* 727 (4-5) (2013) 511–515.
- [5] M. Bender, P.-H. Heenen, P.-G. Reinhard, Self-consistent mean-field models for nuclear structure, *Rev. Mod. Phys.* 75 (1) (2003) 121.
- [6] J.-P. Ebran, E. Khan, T. Nikšić, D. Vretenar, How atomic nuclei cluster, *Nature* 487 (7407) (2012) 341.
- [7] J. Cui, X. Zhou, A beyond-mean-field model for hypernuclei with skyrme-type  $n$  interaction, *Prog. Theor. Exp. Phys* 9 (2017) 093D04.
- [8] Y. Kanada-En'yo, The structure of ground and excited states of  $^{12}\text{C}$ , *Prog. Theor. Phys.* 117 (4) (2007) 655.
- [9] M. Chernykh, H. Feldmeier, T. Neff, P. von Neumann-Cosel, A. Richter, Structure of the Hoyle state in  $^{12}\text{C}$ , *Phys. Rev. Lett.* 98 (3) (2007) 032501.
- [10] M. Freer, H. Horiuchi, Y. Kanada-En'yo, D. Lee, U. Meißner, Microscopic clustering in light nuclei, *Rev. Mod. Phys.* 90 (3) (2018) 035004.
- [11] D. J. Marin-Lambarri, R. Bijker, M. Freer, M. Gai, T. Kokalova, D. J. Parker, C. Wheldon, Evidence for triangular  $d$  3 h symmetry in  $^{12}\text{C}$ , *Phys. Rev. Lett.* 113 (1) (2014) 012502.
- [12] B. Pritychenko, M. Birch, B. Singh, M. Horoi, Tables of E2 transition probabilities from the first  $2^+$  states in even-even nuclei, *At. Data Nucl. Data Tables* 107 (2016) 1–139.
- [13] A. D'Alessio, T. Mongelli, M. Arnold, S. Bassauer, J. Birkhan, I. Brandherm, M. Hilcker, T. Hüther, J. Isaak, L. Jürgensen, et al., Precision measurement of the E2 transition strength to the  $2^+$  state of  $^{12}\text{C}$ , *Phys. Rev. C* 102 (1) (2020) 011302.
- [14] R. H. Helm, Inelastic and elastic scattering of 187-MeV electrons from selected even-even nuclei, *Phys. Rev.* 104 (5) (1956) 1466.
- [15] P. Strehl, Untersuchung von  $0^+ - 0^+$ -Übergängen in  $^{12}\text{C}$ ,  $^{24}\text{Mg}$ ,  $^{28}\text{Si}$ ,  $^{32}\text{S}$  und  $^{40}\text{Ca}$  durch unelastische Elektronenstreuung, *Zeitschrift für Physik A Hadrons and nuclei* 234 (5) (1970) 416.
- [16] H. Crannell, T. A. Griffy, L. R. Suelzle, M. R. Yearian, A determination of the transition widths of some excited states in  $^{12}\text{C}$ , *Nucl. Phys. A* 90 (1) (1967) 152.
- [17] H. L. Crannell, T. A. Griffy, Determination of radiative transition widths of excited states in  $^{12}\text{C}$ , *Phys. Rev.* 136 (6B) (1964) B1580.
- [18] B. John, Y. Tokimoto, Y. Lui, H. L. Clark, X. Chen, D. H. Youngblood, Isoscalar electric multipole strength in  $^{12}\text{C}$ , *Phys. Rev. C* 68 (1) (2003) 014305.
- [19] A. Kuronen, J. Räsänen, J. Keinonen, P. Tikkanen, E. Rauhala, Electronic stopping power for  $^7\text{Li}$ ,  $^{11}\text{B}$ ,  $^{12}\text{C}$ ,  $^{14}\text{N}$  and  $^{16}\text{O}$  at energies 0.4 to 2.1 MeV/nucleon in Ta and Au, and for  $^{12}\text{C}$  at energies 0.4, 0.8 and 1.4 MeV/nucleon in 18 elemental solids, *Nucl. Instrum. Methods Phys. Res., Sec. B* 35 (1) (1988) 1.
- [20] Lu Xiting, Ban Yong, Liu Hongtao, Liu Jiarui, Zheng Zhongshuang, Zhang Qichu, DSA measurement using heavy ion reactions on the small tandem accelerator, *Nucl. Instrum. Methods Phys. Res., Sec. A* 272 (3) (1988) 909–912.
- [21] R. B. Begzhanov, F. S. Akilov, A. K. Khalikov, M. S. Rakhmankulov, Lifetimes of excited states of several light nuclei obtained by a new method of Doppler broadening of  $\gamma$ -lines, *Izv. Akad. Nauk Uzb. SSR, Ser. Fiz.-Mat. Nauk* 59 (4) (1976).
- [22] P. M. Cockburn, W. J. Stark, R. W. Krone, Lifetime measurements from the analysis of Doppler-broadened shapes, *Phys. Rev. C* 1 (5) (1970) 1757.
- [23] F. Riess, P. Paul, J. B. Thomas, S. S. Hanna, Lifetimes of levels in  $^{12,13}\text{C}$  and  $^{13}\text{N}$ , *Phys. Rev.* 176 (4) (1968) 1140.
- [24] A. L. Catz, S. Amiel, Study of lifetimes of nuclear levels by Doppler broadening attenuation using a Ge(Li) gamma-ray spectrometer, *Nucl. Phys. A* 92 (1) (1967) 222.
- [25] E. K. Warburton, J. W. Olness, K. W. Jones, C. Chasman, R. A. Ristinen, D. H. Wilkinson, Lifetime determinations for nuclei  $A=10, 11$ , and  $12$  from gamma-ray Doppler shifts, *Phys. Rev.* 148 (3) (1966) 1072.
- [26] S. Devons, Electromagnetic lifetimes and properties of nuclear states, *National Academy of Sciences* 974 (1962) 86.
- [27] J. Fagot, R. Lucas, H. Nifenecker, M. Schneeberger, Faisceau  $\gamma$  quasi monochromatique à énergie variable, *Nucl. Instrum. Methods* 95 (3) (1971) 421–427.
- [28] Adopted  $B(E2)$  values, Available online from: <https://www.nndc.bnl.gov/be2/index.jsp> (2022).
- [29] P. Navrátil, J. P. Vary, B. R. Barrett, Properties of  $^{12}\text{C}$  in the ab initio nuclear shell model, *Phys. Rev. Lett.* 84 (25) (2000) 5728.
- [30] C. Forsssén, R. Roth, P. Navrátil, Systematics of  $2^+$  states in C isotopes from the no-core shell model, *J. Phys. G* 40 (5) (2013) 055105.
- [31] R. Machleidt, D. R. Entem, Chiral effective field theory and nuclear forces, *Phys. Rep.* 503 (1) (2011) 1–75.
- [32] K. Alder, A. Winther, *Electromagnetic Excitation*, North-Holland, Amsterdam, 1975.
- [33] M. K. Raju, J. N. Orce, P. Navrátil, G. C. Ball, T. E. Drake,

- S. Triambak, G. Hackman, C. J. Pearson, K. J. Abrahams, E. H. Akakpo, et al., Reorientation-effect measurement of the first  $2^+$  state in  $^{12}\text{C}$ : Confirmation of oblate deformation, *Phys. Lett. B* 777 (2018) 250.
- [34] W. J. Vermeer, M. T. Esat, J. A. Kuehner, R. H. Spear, A. M. Baxter, S. Hinds, Electric quadrupole moment of the first excited state of  $^{12}\text{C}$ , *Phys. Lett. B* 122 (1) (1983) 23.
- [35] J. Saiz-Lomas, M. Petri, I. Lee, I. Syndikus, S. Heil, J. Allmond, L. Gaffney, J. Pakarinen, H. Badran, T. Calverley, et al., The spectroscopic quadrupole moment of the  $2^+$  state of  $^{12}\text{C}$ : A benchmark of theoretical models, *Phys. Lett. B* 845 (2023) 138114.
- [36] O. Häusser, Coulomb reorientation, in: *Pure and Applied Physics*, Vol. 40, Elsevier, 1974, p. 55.
- [37] J. de Boer, J. Eichler, *The Reorientation Effect*, Springer US, Boston, MA, 1968, Ch. 1, p. 52.
- [38] K. Nakai, F. S. Stephens, R. M. Diamond, Quadrupole moments of the first excited states in  $^{20}\text{Ne}$  and  $^{22}\text{Ne}$ , *Nucl. Phys. A* 150 (1) (1970) 114–128.
- [39] R. Roth, Importance truncation for large-scale configuration interaction approaches, *Phys. Rev. C* 79 (6) (2009) 064324.
- [40] R. Machleidt, High-precision, charge-dependent Bonn nucleon-nucleon potential, *Phys. Rev. C* 63 (2) (2001) 024001.
- [41] Y. Abgrall, B. Morand, E. Caurier, Multipole deformations, static quadrupole moments and electromagnetic transitions in light nuclei, *Nucl. Phys. A* 192 (2) (1972) 372–390.
- [42] R. H. Bassel, B. A. Brown, R. Lindsay, N. Rowley,  $0^+ (gs) \rightarrow 2^+ (4.44 \text{ MeV})$  transition density in  $^{12}\text{C}$ , *J. Phys. G* 8 (9) (1982) 1215.
- [43] S. Cohen, D. Kurath, Effective interactions for the  $1p$  shell, *Nucl. Phys.* 73 (1) (1965) 1–24.
- [44] C. Yuan, T. Suzuki, T. Otsuka, F. Xu, N. Tsunoda, Shell-model study of boron, carbon, nitrogen, and oxygen isotopes with a monopole-based universal interaction, *Phys. Rev. C* 85 (2012) 064324.
- [45] H. Kitagawa, Shell model study of the quadrupole moments in light mirror nuclei, *Prog. Theor. Phys.* 102 (5) (1999) 1015–1026.
- [46] H. Sagawa, X.-R. Zhou, X. Z. Zhang, T. Suzuki, Deformations and electromagnetic moments in carbon and neon isotopes, *Phys. Rev. C* 70 (5) (2004) 054316.
- [47] G. Dollinger, T. Faestermann, *Physics at the Munich tandem accelerator laboratory*, *Nucl. Phys. News* 28 (1) (2018) 5.
- [48] W. A. Mayer, J. Koenig, H. J. Körner, D. Pereira, K. E. Rehm, H. J. Scheerer, *Entwicklung eines Fokalebenenendetektors für mittelschwere Ionen*, *Jahresbericht BL* (1981) 142.
- [49] R. Lutter, O. Schaile, K. Schoffel, K. Steinberger, P. Thirolf, B. C., MARaBOU-A MBS and ROOT based online/offline utility, *IEEE Transactions on Nuclear Science* (1999).
- [50] J. R. Beene, R. M. DeVries, Particle line shapes in heavy-ion reactions, *Phys. Rev. Lett.* 37 (15) (1976) 1027.
- [51] T. Czosnyka, D. Cline, C. Wu, *Gosia manual*, *Bull. Am. Phys. Soc* 28 (1983) 745.
- [52] W. J. Vermeer, M. T. Esat, J. A. Kuehner, R. H. Spear, A. M. Baxter, S. Hinds, Coulomb excitation of the  $2.615 \text{ MeV} (3^-)$  and  $4.086 \text{ MeV} (2^+)$  states of  $^{208}\text{Pb}$ , *Austr. J. Phys.* 37 (2) (1984) 123.
- [53] D. Goutte, J. B. Bellicard, J. M. Cavedon, B. Frois, M. Huet, P. Leconte, P. X. Ho, S. Platchkov, J. Heisenberg, J. Lichtenstadt, et al., Determination of the transition charge density of the octupole vibration in  $^{208}\text{Pb}$ , *Phys. Rev. Lett.* 45 (20) (1980) 1618.
- [54] R. H. Spear, W. J. Vermeer, M. T. Esat, J. A. Kuehner, A. M. Baxter, S. Hinds, An improved determination of the quadrupole moment of the first excited state of  $^{208}\text{Pb}$ , *Phys. Lett. B* 128 (1-2) (1983) 29–32.
- [55] O. Häusser, A. B. McDonald, T. K. Alexander, A. J. Ferguson, R. E. Warner, E1 polarization in Coulomb excitation of  $^7\text{Li}$ , *Nucl. Phys. A* 212 (3) (1973) 613.
- [56] O. Häusser, A. B. McDonald, T. K. Alexander, A. J. Ferguson, R. E. Warner, Nuclear polarizability of  $^7\text{Li}$  from coulomb excitation, *Phys. Lett. B* 38 (2) (1972) 75.
- [57] J. A. Kuehner, R. H. Spear, W. J. Vermeer, M. T. Esat, A. M. Baxter, S. Hinds, A measurement of the giant-dipole-resonance contribution to the Coulomb excitation of  $^{17}\text{O}$ , *Phys. Lett. B* 115 (6) (1982) 437.
- [58] J. N. Orce, New formulas for the  $(-2)$  moment of the photoabsorption cross section,  $\sigma_{-2}$ , *Phys. Rev. C* 91 (6) (2015) 064602.
- [59] J. S. Levinger, Migdal's and Khokhlov's calculations of the nuclear photoeffect, *Phys. Rev.* 107 (2) (1957) 554.
- [60] J. N. Orce, C. Ngwetssheni, Electric dipole polarizability of low-lying excited states in atomic nuclei, *J. Phys. G* 51 (7) (2024) 075105.
- [61] E. K. Warburton, J. Weneser, *Electromagnetic properties*, Vol. Chapter 4, Science Direct, 1969.
- [62] G. Racah, Theory of complex spectra, *Phys. Rev.* 62 (9-10) (1942) 438.
- [63] S. K. Bogner, R. J. Furnstahl, R. J. Perry, Similarity renormalization group for nucleon-nucleon interactions, *Phys. Rev. C* 75 (6) (2007) 061001.
- [64] D. R. Entem, R. Machleidt, Y. Nosyk, High-quality two-nucleon potentials up to fifth order of the chiral expansion, *Phys. Rev. C* 96 (2) (2017) 024004.
- [65] D. R. Entem, R. Machleidt, Accurate charge-dependent nucleon-nucleon potential at fourth order of chiral perturbation theory, *Phys. Rev. C* 68 (4) (2003) 041001.
- [66] V. Somà, P. Navrátil, F. Raimondi, C. Barbieri, T. Duguet, Novel chiral Hamiltonian and observables in light and medium-mass nuclei, *Phys. Rev. C* 101 (1) (2020) 014318.
- [67] P. Gysbers, G. Hagen, J. D. Holt, G. R. Jansen, T. D. Morris, P. Navrátil, T. Papenbrock, S. Quaglioni, A. Schwenk, S. R. Stroberg, et al., Discrepancy between experimental and theoretical  $\beta$ -decay rates resolved from first principles, *Nature Physics* 15 (5) (2019) 428–431.
- [68] K. Kravvaris, P. Navrátil, S. Quaglioni, C. Hebborn, G. Hupin, Ab initio informed evaluation of the radiative capture of protons on  $^7\text{Be}$ , *Phys. Lett. B* 845 (2023) 138156.
- [69] L. Giralda, A. Kievsky, M. Viviani, Subleading contributions to the three-nucleon contact interaction, *Phys. Rev. C* 84 (1) (2011) 014001.
- [70] M. A. Marchisio, N. Barnea, O. G., Efficient method for Lorentz integral transforms of reaction cross sections, *Few-Body Systems* 33 (4) (2003) 259.
- [71] F. C. Barker, C. L. Woods, Investigation of E1 strength in Coulomb excitation of light nuclei, *Austr. J. Phys.* 42 (3) (1989) 233–256.
- [72] Y. Hao, P. Navrátil, E. B. Norrgard, M. Iliaš, E. Eliav, R. G. E. Timmermans, V. V. Flambaum, A. Borschevsky, Nuclear spin-dependent parity-violating effects in light polyatomic molecules, *Phys. Rev. A* 102 (5) (2020) 052828.
- [73] P. Froese, P. Navrátil, Ab initio calculations of electric dipole moments of light nuclei, *Phys. Rev. C* 104 (2) (2021) 025502.
- [74] M. Gennari, M. Drissi, M. Gorchtein, P. Navrátil, C.-Y. Seng, An ab initio recipe for taming nuclear-structure dependence of  $V_{\text{ud}}$ : the  $^{10}\text{C} \rightarrow ^{10}\text{B}$  superallowed transition, *arXiv preprint arXiv:2405.19281* (2024).
- [75] E. G. Fuller, Photoneuclear reaction cross sections for  $^{12}\text{C}$ ,  $^{14}\text{N}$  and  $^{16}\text{O}$ , *Phys. Rep.* 127 (3) (1985) 185.
- [76] J. Ahrens, H. Borchert, K. H. a. Czock, H. B. Eppler, H. Gimm, H. Gundrum, M. Kröning, P. Riehn, G. S. Ram, A. Zieger, et al.,

- Total nuclear photon absorption cross sections for some light elements, *Nucl. Phys. A* 251 (3) (1975) 479.
- [77] J. N. Orce, C. Ngwetsheni, B. A. Brown, Global trends of the electric dipole polarizability from shell-model calculations, *Phys. Rev. C* 108 (2023) 044309.
- [78] E. K. Warburton, B. A. Brown, Effective interactions for the 0p1s0d nuclear shell-model space, *Phys. Rev. C* 46 (3) (1992) 923.
- [79] S. Raman, C. Nestor Jr, P. Tikkanen, Transition probability from the ground to the first-excited 2+ state of even-even nuclides, *At. Data Nucl. Data Tables* 78 (1) (2001) 1–128.
- [80] M. Wang, W. J. Huang, F. G. Kondev, G. Audi, S. Naimi, The AME 2020 atomic mass evaluation (ii). tables, graphs and references, *Chinese Phys. C* 45 (3) (2021) 030003.
- [81] K. Hebeler, S. K. Bogner, R. J. Furnstahl, A. Nogga, A. Schwenk, Improved nuclear matter calculations from chiral low-momentum interactions, *Phys. Rev. C* 83 (2011) 031301.
- [82] A. Bohr, B. R. Mottelson, *Nuclear Structure*, World Scientific Publishing Company, 1998.
- [83] A. DeShalit, H. Feshbach, *Theoretical nuclear physics*, New York, NY (USA); John Wiley and Sons Inc., 1990.
- [84] W. B. He, Y. G. Ma, X. G. Cao, X. Z. Cai, G. Q. Zhang, et al., Giant dipole resonance as a fingerprint of  $\alpha$  clustering configurations in  $^{12}\text{C}$  and  $^{16}\text{O}$ , *Phys. Rev. Lett.* 113 (3) (2014) 032506.
- [85] M. Frosini, T. Duguet, J. P. Ebran, V. Somà, Multi-reference many-body perturbation theory for nuclei, *Eur. Phys. J. A* 58 (4) (2022) 1–28.
- [86] P. Marević, J.-P. Ebran, E. Khan, T. Nikšić, D. Vretenar, Cluster structures in  $^{12}\text{C}$  from global energy density functionals, *Phys. Rev. C* 99 (3) (2019) 034317.
- [87] P. Navrátil, S. Quaglioni, G. Hupin, C. Romero-Redondo, A. Calci, Unified ab initio approaches to nuclear structure and reactions, *Phys. Scripta* 91 (5) (2016) 053002.
- [88] K. Kravvaris, S. Quaglioni, G. Hupin, P. Navrátil, Ab initio framework for nuclear scattering and reactions induced by light projectiles, *Phys. Lett. B* 856 (2024) 138930.
- [89] S. R. Stroberg, J. Henderson, G. Hackman, P. Ruotsalainen, G. Hagen, J. D. Holt, Systematics of E2 strength in the sd shell with the valence-space in-medium similarity renormalization group, *Phys. Rev. C* 105 (3) (2022) 034333.
- [90] J. Henderson, G. Hackman, P. Ruotsalainen, J. D. Holt, S. R. Stroberg, C. Andreoiu, G. C. Ball, N. Bernier, M. Bowry, R. Caballero-Folch, et al., Coulomb excitation of the  $|T_2\rangle=1/2$ ,  $A=23$  mirror pair, *Phys. Rev. C* 105 (3) (2022) 034332.